Terrestrial environmental change across the onset of the PETM and the associated impact on biomarker proxies: a cautionary tale

Gordon N. Inglis[a,b], Alexander Farnsworth[b,c], Margaret E. Collinson[d], Matthew J. Carmichael[a,b,c], B. David A. Naafs[a,b], Daniel J. Lunt[b,c], Paul J Valdes[b,c], and Richard D. Pancost[a,b]

[a] Organic Geochemistry Unit, School of Chemistry, and School of Earth Sciences, University of Bristol, Bristol, UK

[b] Cabot Institute, University of Bristol, Bristol, UK

[c] BRIDGE, School of Geographical Sciences, University of Bristol, UK

[d] Department of Earth Sciences, Royal Holloway University of London, UK

Corresponding author: Gordon N. Inglis

Email: gordon.inglis@bristol.ac.uk. Telephone: +44 (0)117 954 6395

Abstract:

The Paleocene-Eocene Thermal Maximum (PETM; ~ 56 million years ago (Ma) is the most severe carbon cycle perturbation event of the Cenozoic. Although the PETM is associated with warming in both the surface (~up to 8°C) and deep ocean (~up to 5°C), there are relatively few terrestrial temperature estimates from the onset of this interval. The associated response of the hydrological cycle during the PETM is also poorly constrained. Here, we use biomarker proxies (informed by models) to reconstruct temperature and hydrological change within the Cobham Lignite (UK) during the latest Paleocene and early PETM. Previous work at this site indicates warm terrestrial temperatures during the very latest Paleocene (ca. 22 to 26°C). However, biomarker temperature proxies imply cooling during the onset of the PETM (ca. 5 to 11°C cooling), inconsistent with other local, regional and global evidence. This coincides with an increase in pH (ca. 2 pH units with pH values > 7), enhanced waterlogging, a major reduction in fires and the development of areas of open water within a peatland environment. This profound change in hydrology and environment biases biomarker temperature proxies, including the branched GDGT paleothermometer. This serves as a cautionary tale on the danger of attempting to interpret biomarker proxy records without a wider understanding of their environmental context.

Keywords: lignite, biomarkers, GDGTs, hydrology, Eocene, peat

1. Introduction

The Paleocene-Eocene Thermal Maximum (PETM; ca. 56 million years ago) is a rapid global warming event associated with the release of ^{13}C-depleted carbon into the ocean-atmosphere system. During the PETM, the deep ocean warmed by ~5°C (Tripati and Elderfield, 2005; Zachos et al., 2008a) and sea surface temperatures increased by up to 8°C (Aze et al., 2014; Frieling et al., 2017; Frieling et al., 2014; Schoon et al., 2015; Sluijs et al., 2011; Sluijs et al., 2006; Sluijs et al., 2014; Zachos et al., 2006). During the same interval, continental temperatures increased significantly (ca. 4 to 7°C) (Fricke and Wing, 2004; Gehler et al., 2016; Secord et al., 2010; Wing et al., 2005). There is other evidence for increasing terrestrial temperatures during the PETM, including floral turnover (Schouten et al., 2007; Wing et al., 2005), enhanced insect herbivory (Currano et al., 2008) and mammalian (Secord et al., 2012) and soil faunal dwarfing (Smith et al., 2009). However, our understanding of continental temperature change during the PETM remains restricted to a few, well-sampled regions (primarily western North America) and additional records are required to fully evaluate climate model simulations.

Continental temperatures are also important because they exert a first-order control upon the hydrological cycle. During the PETM, proxies and models indicate that the hydrological cycle exhibits a globally ‘wet-wetter, dry-drier’ style response (Carmichael et al., 2017). However, there is significant regional and temporal variability in both proxy and model data. For example, high-latitude and coastal settings are generally characterised by stable and/or increasing rainfall, with proxy evidence for both enhanced terrigenous sediment flux to marginal marine sediments (John et al., 2008) and enhanced chemical weathering (Dickson et al., 2015; Ravizza et al., 2001). In contrast, mid-to-low latitude and continental interior settings are

typically characterised by decreasing rainfall but an increase in extreme precipitation rates (Carmichael et al., 2018; Handley et al., 2012; Schmitz and Pujalte, 2007). Perturbations to the hydrological cycle also impacted vegetation patterns (Collinson et al., 2009; Jaramillo et al., 2010) and various biogeochemical cycles (e.g. methane cycling; Pancost et al., 2007), and may have played an important role in maintaining the warmth of the PETM (Zachos et al., 2008b) and in the subsequent recovery phase (Gutjahr et al., 2017).

To reconstruct temperature and hydrological change during the PETM, we investigate the biomarker distributions within an immature lignite seam from Cobham, Kent, UK (~48°N palaeolatitude). The Cobham Lignite Bed is inferred to represent an ancient continental mire system and is characterised by a negative carbon isotope excursion characteristic at the PETM onset (Collinson et al., 2003; Pancost et al., 2007; see Collinson et al., 2009 for details on age model). We consider our new results in the context of previously published indicators of vegetation and hydrological change (Collinson et al., 2003; Steart et al., 2007; Collinson et al., 2009; Collinson et al., 2013) and new climate model simulations to develop a holistic and nuanced understanding of paleoenvironmental change in northern Europe across the onset and during the early PETM. Our results serve as a cautionary tale on interpreting biomarker proxies without a wider understanding of their environmental context.

2. Methods

2.1.1. Sample site

The Cobham Lignite Bed was deposited in a low-lying freshwater setting very near sea-level (~48 °N palaeolatitude). The Cobham Lignite Bed is underlain by a sand and

mud unit (shallow marine; S&M). The Cobham Lignite Bed comprises a thin clay layer (<10 cm) at the base, overlain by a charcoal-rich lower laminated lignite (ca. 43 cm thick; lower LL). This is overlain by a charcoal-poor upper laminated lignite (ca. 2 cm thick; upper LL), a middle clay layer (MCL < 10 cm thick) and a charcoal-poor blocky lignite (ca. 130 cm thick; BL). The Woolwich Shell Beds (marginal marine/lagoonal, containing the *Apectodinium* acme; WSB) overly the Cobham Lignite (Collinson et. al. 2009).

2.1.2. Age control

The Cobham Lignite Bed is underlain by the Upnor Formation, which at a nearby site is dated as latest Palaeocene by means of the occurrence of calcareous nannoplankton zone NP9 and magnetochron C25n in its lower part (Collinson et al., 2009). A negative carbon isotope excursion (CIE) of ~ 1.5 ‰ is present near the top of the charcoal-poor upper laminated lignite (54.45 cm), slightly below the middle clay layer. This is interpreted as being the negative CIE characteristic of the PETM (Collinson et al., 2003; 2007; 2009). As such, we interpret the uppermost laminated lignite (54.45 to 57.6cm), middle clay layer (57.6 to 65.3 cm) and blocky lignite (65.3 to 194.8 cm) to reflect PETM age. Based on a peat to lignite compaction ratios, the blocky lignite (65.3 to 194.8 cm) is likely to have accumulated as peat during 4–12 kyr (range 1–42 kyr) (Collinson et al., 2009) and thus represents only the early part of the PETM. The shallow-marine Woolwich Formation, which overlies the Cobham Lignite Bed at Cobham, contains the *Apectodinum* acme indicating that it is also within the PETM. For a full description of the stratigraphy, see Collinson et al. (2009).

122 *2.2. Lipid extraction*

123 The current study utilised aliquots of total lipid extract (TLE) originally prepared
124 by Pancost et al. (2007) and which had been stored dry and frozen (-20 °C). We focus
125 here exclusively on the lignite sediments (Supplementary Information). Briefly, the
126 powdered samples were extracted by sonication with a sequence of increasingly
127 polar solvents (four times with dichloromethane (DCM), four times with
128 DCM/methanol (MeOH) (1:1, *v/v)* and three times with MeOH). The total lipid
129 extracts were separated into three fractions using a column packed with (activated)
130 alumina by elution with hexane (apolar fraction), hexane/DCM (9:1 v/v) and
131 DCM/MeOH (1:2 v/v; polar fraction). The polar fraction, containing the GDGTs, was
132 dissolved in hexane/*iso*-propanol (99:1, v/v) and passed through a 0.45 µm PTFE filter.

133

134 *2.3. Analytical methods*

135 Hydrocarbon fractions were analysed using a Thermoquest Finnigan Trace GC
136 interfaced to a Thermoquest Finnigan Trace MS. This was achieved using a fused
137 silica capillary column (50 m × 0.32 mm) coated with CP-Sil-5 (film thickness
138 0.12 µm) and via the following temperature programme: 40 °C to 140 °C at
139 20 °C min^{-1}, then to 300 °C at 4 °C min^{-1}, maintained at 300 °C for 22 min. Polar
140 fractions were analysed by high performance liquid chromatography/atmospheric
141 pressure chemical ionisation – mass spectrometry (HPLC/APCI-MS). Samples were
142 analysed following Hopmans et al. (2016). Normal phase separation was achieved
143 using two Waters Acquity UPLC BEH Hilic columns (2.1 x 150 mm; 1.7 µm i.d.) with a
144 flow rate of 0.2 ml. min^{-1}. Samples were eluted isocratically with 78% A and 18% B for
145 25 min followed by a linear gradient to 35% B over 25 minutes, then a linear gradient

to 100% B in 30 minutes, where A = hexane and B = hexane:IPA (9:1, v/v) (Hopmans et al., 2016). Injection volume was 15 µL, typically from 100 µL. Analyses were performed using selective ion monitoring mode (SIM) to increase sensitivity and reproducibility (*m/z* 1302, 1300, 1298, 1296, 1294, 1292, 1050, 1048, 1046, 1036, 1034, 1032, 1022, 1020, 1018, 744, and 653).

2.4. Biomarker proxies

2.4.1. Biomarker-based temperature proxies

Branched glycerol dialkyl glycerol tetraethers (brGDGTs) are membrane lipids produced by Bacteria (likely Acidobacteria; Sinninghe Damsté et al., 2018). The distribution of brGDGTs in peats is influenced by mean annual near-surface air temperature (MAAT), with the degree of methylation decreasing as temperature increases (Weijers et al., 2007; Naafs et al., 2017). This is captured in the methylation of branched tetraether (MBT'_{5ME}) index (De Jonge et al., 2014):

(1) $MBT'_{5ME} = (Ia + Ib + Ic)/(Ia + Ib + Ic + IIa + IIb + IIc + IIIa)$

For application to peats and lignites MBT'_{5ME} is translated to MAAT using the peat-specific calibration (Naafs et al., 2017):

(2) $MAAT_{peat} = 52.18 * MBT'_{5ME} – 23.05$ ($n = 94$, $r^2 = 0.76$; RMSE = 4.7°C)

Roman numerals refer to individual GDGT structures shown in the Supplementary Information (Figure S1). In brief, I, II and III represent the tetra-, penta- and hexamethylated components, respectively, and a, b and c represent the brGDGTs bearing 0, 1 or 2 cyclopentane moieties. Penta- and hexamethylated brGDGTs can be

methylated at the C-5 position or C-6 position on the alkyl chain. The latter are indicated by an apostrophe (e.g. IIa' – see equation (7)). Note that samples from the lower laminated lignite (i.e. pre-PETM; n = 7) were previously analysed for branched GDGTs. For more details, see Naafs et al., (2018b).

Recent work has demonstrated that the distribution of bacterial-derived branched glycerol monoalkyl glycerol tetraethers (brGMGTs) can also be influenced by MAAT, with the degree of methylation decreasing as temperature increases (Naafs et al., 2018a). This is captured in the H-MBT$_{acyclic}$ index:

(3) H-MBT$_{acyclic}$ = (H-Ia) / ([H-Ia] + [H-IIa] + [H-IIIa])

In addition to brGDGTs and brGMGTs produced by Bacteria, peats also contain a wide variety of isoprenoidal (iso)GDGTs, produced by Archaea (Weijers et al., 2004). Of these compounds, isoGDGT-5 occurs exclusively within acidic (pH < 5.1) tropical (> 19°C) peats (Naafs et al., 2018b). The relative abundance of isoGDGT-5 is captured using the following index:

(4) %GDGT-5 = (isoGDGT-5)/(isoGDGT-1 + isoGDGT-2 + isoGDGT-3 + isoGDGT-5)

%GDGT-5 values > 1% are only found in peats with both a MAAT > 19.5°C and pH < 5.1. isoGDGT-4 is excluded from this ratio due to co-elution with crenarchaeol. Note that samples from the lower laminated lignite (i.e. pre-PETM; n = 7) were previously analysed for isoGDGT-5. For more details, see Naafs et al., (2018b).

2.4.2. Biomarker-based pH proxies

In addition to temperature, the distribution of brGDGTs can also be influenced by other environmental parameters, such as pH. For instance, both 5- and 6-methyl brGDGTs are more abundant at higher pH (De Jonge et al., 2014). This is captured in a modified version of the cyclisation of branched tetraether (CBT) index:

(5) CBT_{peat} = log(Ib + IIa' + IIb + IIb' + IIIa')/(Ia + IIa + IIIa)

CBT_{peat} is translated to peat pH using the following equation (Naafs et al., 2017):

(6) pH = 2.49 * CBT_{peat} + 8.07 (n = 51; r^2 = 0.58; RMSE = 0.8)

6-methyl brGDGTs are also more abundant at higher pH (De Jonge et al., 2014; Yang et al., 2015). This is captured in the $IR6_{ME}$ index (Yang et al., 2015):

(7) $IR6_{ME}$ = (IIa' + IIb' + IIc' + IIIa' + IIIb' + IIIc') / (IIa + IIa' + IIb + IIb' + IIc + IIc' + IIIa + IIIa' + IIIb + IIIb' + IIIc + IIIc')

Peat pH can also be reconstructed using the isomerisation of bacterial-derived hopanoids (C_{31} hopane ββ/(ββ+αβ; Pancost et al., 2003). This index is translated to pH using the following equation (Inglis et al., 2018):

(8) pH = 5.22 * (C_{31} hopane ββ/(ββ+αβ) + 3.11 (n = 94, r^2 = 0.64; RMSE = 1.4)

2.5. Modelling simulations

Temperature and precipitation estimates were obtained for the Early Eocene (Ypresian) from an ensemble of coupled atmosphere–ocean GCMs. These simulations include the EoMIP ensemble (Lunt et al., 2012), but also more recent simulations (Inglis et al., 2017; Kiehl and Shields, 2013; Sagoo et al., 2013) (Table 1).

Simulation	CO_2 (relative to pre-industrial)	Reference
HadCM3L	x2, x4, x6	Lunt et al. (2012)
HadCM3L-I	x2, x4	Inglis et al., 2017
HadCM3L-I2	x2, x3, x6	*This paper*
HadCM3L-C	x2, x4	Carmichael et al., (2018)
HadCM3L-V	x6	Inglis et al., 2017
ECHAM	x2	Heinemann et al. (2009)
CCSM3W	x4, x8, x16	Winguth et al. (2010; 2012)
CCSM3H	x2, x4, x8, x16	Huber and Caballero (2011)
CCSM3K	x5	Kiehl and Shields (2013)
GISS	x4, x8, x16	Roberts et al. (2009)
FAMOUS-1	x2	Sagoo et al. (2013)
FAMOUS-2	x2	Sagoo et al. (2013)

Table 1: Summary of model simulations. See the supplementary information and original references for more details.

We also generate new temperature and precipitation estimates using a revised version of HadCM3L, HadCM3L-I2 (Table 1). Using the nomenclature of Valdes et al. (2017) these new model simulations are carried out using the HadCM3L-M2.1aD version of the model. The boundary conditions (paleogeography, solar forcing) representing the Ypresian are the same as in Lunt et al. (2016) but with modifications made to the ozone distribution such that it more closely reproduces modern ozone and consequently surface air temperature values when run under modern conditions. These new simulations were initialised from a previous 10,422 model years fully equilibriated 2x preindustrial CO_2 run of the Ypresian. One simulation was kept constant at 2x preindustrial CO_2 for 1000 model years while the second experiment used elevated 6x preindustrial CO_2 for 1000 model years, and a third simulations used 3x preindustrial CO_2 for 6,000 model years. A mean of the last 50-years is used to produce the climatologies in all 3 simulations. To study changes in occurrence of extreme events, we also include the simulations by Carmichael et al. (2018).

Simulations are performed with atmospheric CO_2 at 2*x* and 4*x* preindustrial concentrations. However, unlike other HadCM3L simulations, precipitation rates were recorded at every model hour for the 99-year run. Within the simulated palaeogeography the nearest land point to the Cobham locality was identified using the Getech Plc. plate model at the mid-point of the appropriate geological stage (Ypresian), which is consistent with the paleogeographies in the HadCM3L-I and HadCM3L-I2 simulations.

3. Results

3.1. Biomarker distributions in Cobham lignite sediments

The branched GDGT (brGDGT) distribution within the lower laminated lignite (4.65 to 43.3 cm) is dominated by tetramethylated brGDGTs (average: 90% of the total brGDGT assemblage; Fig. 1a). Within the upper laminated lignite (54.15 to 55.9 cm), the relative abundance of tetramethylated brGDGTs decreases (average: 78 % of the total brGDGT assemblage). The relative abundance of tetramethylated brGDGTs decreases further within the blocky lignite (average: 65% of the total brGDGT assemblage; 67.5 to 194.8 cm).

The isoprenoidal GDGT (isoGDGT) distribution within lower laminated lignite (4.65 to 43.3 cm) is dominated by GDGTs with 0 to 5 cyclopentane moieties and the abundance of isoGDGT-5 is high (average %GDGT-5: 3.0%). Within the upper laminated lignite (54.15 to 55.9 cm), the abundance of isoGDGT-5 is slightly lower (average %GDGT-5: 2.3%). Within the blocky lignite (67.5 to 194.8 cm), isoGDGT-5 is typically absent (although there are exceptions; e.g. 121.9cm) and the relative

abundance of isoGDGT-0 increases significantly (average: 80% of total isoGDGT assemblage).

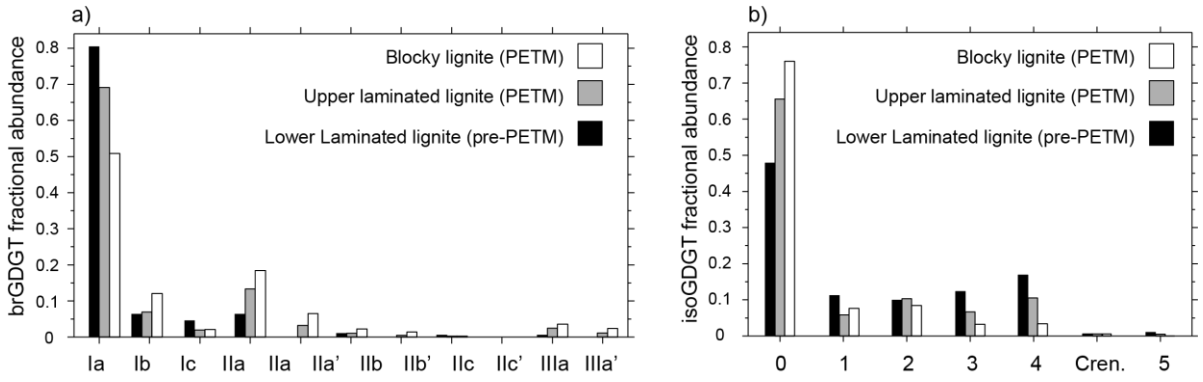

Figure 1: Fractional abundance of (a) branched GDGT and (b) isoprenoidal GDGT lipids within the lower laminated lignite (pre-PETM), upper laminated lignite (PETM onset) and blocky lignite (early PETM)

The Cobham lignite also contains recently identified branched and isoprenoidal glycerol monoalkyl glycerol tetraethers (brGMGTs and isoGMGTs, respectively; Naafs et al., 2018a). The isoGMGT distribution is dominated by isoGMGT-0 throughout (average: 95 % of the total isoGMGT assemblage). The brGMGT distribution within the lower laminated lignite (4.65 to 43.3 cm) is dominated by tetramethylated brGMGTs (average: 85 % of the total brGMGT assemblage; Fig. 1a). Within the upper laminated lignite (54.15 to 55.9 cm), the relative abundance of tetramethylated brGMGTs decreases (average: 75 % of the total brGMGT assemblage). The relative abundance of tetramethylated brGMGTs decreases further within the blocky lignite (average: 65% of the total brGMGT assemblage; 67.5 to 194.8 cm).

The Cobham lignite also contains a range of bacterial-derived C_{27}–C_{32} hopanes and C_{27}–C_{30} hopenes (see Pancost et al., 2007 for full details). The hopanoid distribution within the lower laminated lignite (4.65 to 43.3 cm) is dominated by the (22R)-17α,21β(H)-homohopane (C_{31}) (average: 31% of total hopanoid assemblage).

This is one of the most abundant hopanoids in modern peats and typically dominates the hopane distribution within acidic, ombrotrophic bogs (Inglis et al., 2018). The relative abundance of the (22R)-17α,21β(H)-homohopane (C_{31}) decreases within the upper laminated lignite (average: 15% of total hopanoid assemblage) and the blocky lignite (average: 5% of total hopanoid assemblage). The blocky lignite is dominated by C_{30} hopenes (up to 50% of total hopanoid assemblage).

3.2. MAAT and pH trends in the Cobham Lignite inferred from biomarker proxies

Branched GDGT-derived MAAT estimates from the lower laminated lignite (4.65 to 43.3 cm) are relatively stable and range between ca. 24 and 26 °C (average: 26°C; Naafs et al., 2018b; Fig. 2). Lower MAAT estimates are observed within the upper laminated lignite and blocky lignite. However, see Section 4.1 and 4.2 for further discussion on the validity of these results. CBT_{peat} and C_{31} hopane ββ/(ββ+αβ)-derived pH estimates from the lower laminated lignite (4.65 to 43.3 cm) are relatively low (average: 5.3 and 4.4 pH units, respectively; Fig. 3a-b). CBT_{peat} and C_{31} hopane ββ/(ββ+αβ)-derived pH estimates from the upper laminated lignite increase slightly (average: 6.0 and 4.6 pH units, respectively; Fig. 3a-b). CBT_{peat} and C_{31} hopane ββ/(ββ+αβ)-derived pH estimates increase further within the blocky lignite (average: 6.8 and 6.3 pH units, respectively; Fig. 3a-b).

4. Discussion

4.1. Biomarker-derived temperature estimates across the onset of the PETM

Branched GDGT-derived MAAT estimates from the lower laminated lignite pre-PETM interval (i.e. 4.65 to 54.15 cm) indicate warm terrestrial temperatures (ca. 22 to 26°C; average: 24°C; Naafs et al., 2018b; Fig. 2). Naafs et al., (2018b) also identified the

294 occurrence of isoGDGTs with > 5 cyclopentane moieties during the pre-PETM interval,
295 indicating minimum MAAT estimates of 19°C. High H-MBT$_{acyclic}$ values within the lower
296 laminated lignite (4.65 to 54.15 cm) would also imply elevated terrestrial temperatures
297 (Naafs et al., 2018a). Our biomarker-based temperature estimates also agree with
298 MAAT estimates for the Cobham region simulated by climate model simulations run
299 at high CO_2 concentrations (e.g. HadCM3L 6x PI; CCSM3-H 8x and 16x PI; CCSM3-
300 W 16x PI; Figure 4a; Table 1), in agreement with existing proxy-based CO_2 estimates
301 for the PETM (Hollis et al., 2019). They also agree with climate model simulations
302 which have modified specific model parameters (e.g. CCSM3-K and FAMOUS-1;
303 Figure 4a).

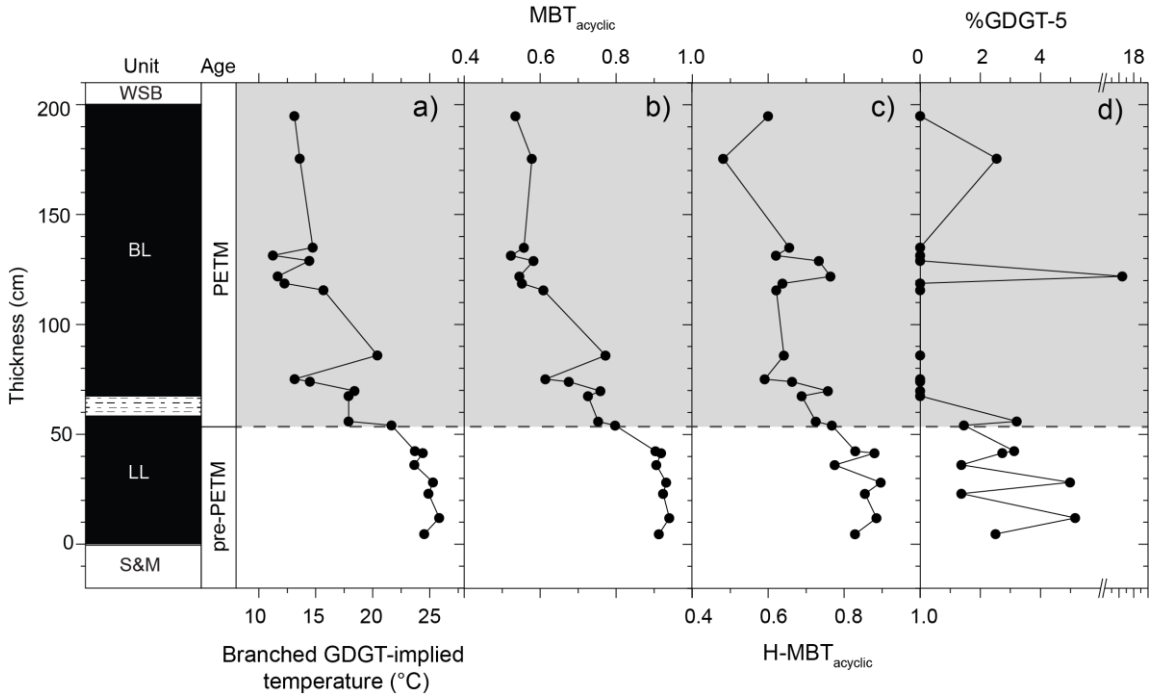

Figure 2: Terrestrial biomarker proxies before, across the onset and during the early part of the PETM at Cobham. a) Branched GDGT-implied MAAT estimates obtained via MAAT$_{peat}$ proxy, b) MBT$_{acyclic}$, c) H-MBT$_{acyclic}$ and d) %GDGT-5. Dashed line corresponds to onset of CIE (54.45 cm). Note that MAATpeat and %GDGT-5 estimates from the charcoal-rich lower laminated lignite (i.e. pre-CIE; n = 7) were published in Naafs et al. (2018).

Branched GDGT-derived MAAT estimates decrease within the PETM-aged upper laminated lignite (54.45 to 55.9 cm) and blocky lignite (67.5 to 194.8 cm), indicating lower terrestrial temperatures at the onset and during the early PETM (ca. 11 to 20°C; average: 15°C; Fig. 2). The PETM-aged blocky lignite (67.5 to 194.8 cm) also contains a lower abundance of isoGDGT-5 (Fig. 2d; but see pH discussion below; section 4.2.3) and lower H-$MBT_{acyclic}$ values (Fig. 2c), both suggesting lower temperatures. Although the absolute temperature estimates agree with MAAT estimates for this region simulated by climate model simulations run at lower CO_2 concentrations (e.g. HadCM3L 2x, 4x PI; ECHAM 2x PI; CCSM3-H 2x and 4x PI, GISS 4x PI; Figure 4a) or that have modified specific model parameters (e.g. HadCM3L-I2 and FAMOUS-2; Figure 4a), for all model simulations in our ensemble with more than one CO_2 concentration (Table 1; Supplementary Information), there is warming at the Cobham location as CO_2 increases.

Decreasing terrestrial temperatures in the upper laminated lignite and the blocky lignite are inconsistent with the presence of the *Apectodidium* acme throughout the overlying Woolwich Shell Beds and the short accumulation time estimated for the BL which demonstrate that the blocky lignite accumulated as peat during the early part of the PETM (Collinson et al 2009). Lower temperatures are also inconsistent with increasing palm pollen in some BL samples (Collinson et al., 2009). Decreasing temperatures are also at odds with the regional response, with proxy evidence for increasing terrestrial temperatures in northern Europe during the PETM (up to 6°C; Schoon et al., 2015). The marine realm also indicates increasing temperatures in northern Europe during the PETM, with evidence for 3 to 4°C of surface ocean warming in both the Bay of Biscay (Bornemann et al., 2014) and the North Sea (Schoon et al., 2015). Decreasing terrestrial temperatures also differ from the global

response during the PETM (Hollis et al., 2019; Jones et al., 2013; McInerney and Wing, 2011). Collectively, this implies that the biomarker-based paleotemperature proxies in the upper laminated lignite and blocky lignite are impacted by non-thermal influences or ecological signals; below we explore what these controls may be.

4.2. Exploring additional controls upon peat-specific biomarker temperature proxies

4.2.1. Vegetation

The lower laminated lignite (pre-PETM) is dominated by fern spores and is rich in charcoal including fern leaf stalks and was interpreted to indicate a fire-prone, low-diversity vegetation (Collinson et al., 2009). In contrast, the upper laminated lignite and blocky lignite (PETM) are characterised by the reduction then loss of ferns and charcoal, an increase in wetland plants (including cupressaceous conifers) and a more varied flowering plant community with palms and eudicots. Although it has been previously argued that changes in vegetation could have influenced the distribution of brGDGTs in peatlands (e.g. Weijers et al., 2011), this was later attributed to the overly strong pH correction in the MBT/CBT proxy (Inglis et al., 2017). Indeed, recent studies within modern peatlands (Naafs et al., 2017) and ancient lignites (Inglis et al., 2017) have indicated that vegetation change is less of a concern than originally inferred by Weijers et al. (2011). As such, we argue that, although there is vegetation change, it is unlikely to have exerted a primary control upon biomarker paleotemperature proxies in the Cobham Lignite.

4.2.2. Lithofacies

352 The Cobham Lignite Bed is characterised by two different lithofacies (laminated vs
353 blocky lignite). The laminated lignite is characterised by repeated (episodic) deposition
354 of charcoal (mostly from local sources, via run-off related local transport; Steart et al.,
355 2007), whereas the overlying blocky lignite is dominated by continuous deposition of
356 non-woody material in a persistent peat-forming environment (Steart et al., 2007).
357 Whilst previous studies have noted subtle differences in brGDGT distributions (and
358 therefore, MAAT estimates; up to 4°C) between different lithofacies (e.g. lignite vs
359 shallow marine sediments; Inglis et al., 2017), a decline in biomarker-based
360 temperature estimates within the Cobham Lignite Bed occurs within the upper
361 laminated lignite (54 to 56 cm; Figure 2) and prior to changes in lithofacies. Therefore,
362 lithofacies are not a primary control upon biomarker paleotemperature proxies in the
363 Cobham Lignite.

364

365 4.2.3. pH, hydrology and presence of open water areas

366 Within the Cobham Lignite Bed, we reconstruct pH using two independent, peat-
367 specific pH proxies: 1) CBT_{peat}, based upon the cyclisation of brGDGTs (Naafs et al.,
368 2017), and 2) the C_{31} hopane ββ/(αβ+ββ) index, based upon the isomerisation of C_{31}
369 hopanes (Inglis et al., 2018). Within the lower laminated lignite (pre-PETM), brGDGT-
370 and hopanoid-derived pH estimates (pH: ca. 4 to 5.5) are low and indicate acidic
371 conditions (Fig. 3). The occurrence of isoGDGT-5 (> 1%; Fig. 2d), the absence of 6-
372 methyl brGDGTs (IR_{6ME} < 0.01; Fig. 3c) and the dominance of the C_{31} αβ hopane
373 provides additional evidence for acidic conditions within the lower laminated lignite.
374 We observe a remarkable increase in hopanoid- and brGDGT-derived pH estimates
375 within the upper laminated lignite (0.5 pH unit) and especially the blocky lignite (ca. 2
376 pH units to pH values > 7.5; Fig. 3). The upper laminated lignite and blocky lignite also

contain a higher abundance of pH-sensitive 6-methyl brGDGTs (average IR_{6ME}: 0.23 and 0.29, respectively; Fig. 3) and a lower abundance of the C_{31} αβ hopane. This indicates a profound change in the environment during the onset and early PETM and provides an alternative explanation for the decrease in the abundance of isoGDGT-5 (see 4.1; Naafs et al., 2018b).

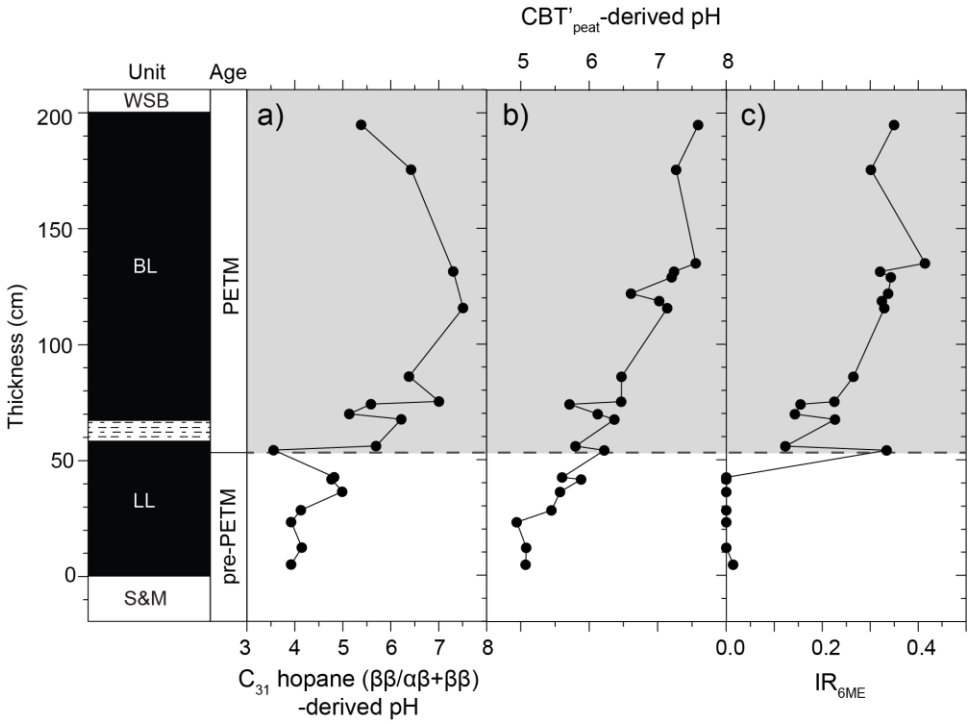

Figure 3: Peat pH before, across the onset and during the early part of the PETM at Cobham, a) C_{31} hopane (ββ/αβ+ββ)-derived pH estimates, b) CBT_{peat}-derived pH estimates, b c) IR_{6ME} (the ratio between 5- and 6-methyl brGDGTs. High values imply higher pH). Dashed line corresponds to onset of CIE.

An increase in pH values within the onset and early PETM implies changes in local hydrology, supported by other hydrological and botanical indicators at Cobham (UK). For example, the blocky lignite is characterised by an increased percentage of *Inaperturopollenites* pollen (representing swamp-dwelling cupressaceous conifers) and *Sparganiaceaepollenites* pollen (representing marginal aquatic

387 monocotyledonous angiosperm herbs), indicating the development of waterlogged
388 swamp environments (Collinson et al., 2009). The base of the blocky lignite also
389 includes the unusual co-occurrence of two genera of freshwater, free-floating water
390 plants, the heterosporous ferns *Salvinia* and *Azolla* (Collinson et al., 2013). There is
391 also the loss of wildfires, with both the upper laminated lignite and blocky lignite having
392 a significant reduction in, or loss of, both macroscopic and microscopic charcoal
393 (Collinson et al., 2009).

394 Taken together, the evidence indicates enhanced waterlogging during the
395 onset of the PETM and the development a persistent peatland with patches of open
396 water. The development of open water conditions is likely to be associated with the
397 input of brGDGTs from aquatic sources (as observed in lakes and ponds; e.g. Colcord
398 et al., 2015; Huguet et al., 2015; Tierney and Russell, 2009; Weber et al., 2018).
399 Aquatic brGDGTs can reflect near-bottom water temperatures (Weber et al., 2018)
400 and application of mineral soil or peat calibrations in modern lacustrine settings
401 consistently yields colder-than-predicted temperatures (up to 10°C in modern
402 systems; Tierney et al., 2010; Zink et al., 2010). The input of GGDTs from aquatic
403 sources can therefore explain the apparent cooling in our brGDGT-derived
404 temperature estimates during the onset of the PETM. This also indicates that the
405 brGDGT paleothermometer in terrestrial archives should not be employed in settings
406 where major changes in pH and hydrology took place. Future work aiming to determine
407 palaeotemperatures would therefore benefit from accompanying proxy-based pH
408 reconstructions based on the distribution of hopanes (Inglis et al., 2018) or branched
409 glycerol dialkyl glycerol tetraethers (brGDGTs) (Naafs et al., 2017) or alternative
410 palaeohydrological indicators (e.g. *n*-alkane δ^2H values; (Sachse et al., 2012)).

411

4.3. A shift towards wetter conditions in northern Europe during the PETM

Our data – as well as previously published proxy evidence – suggests a shift towards wetter conditions during the PETM at Cobham (see section 4.2). To test these observations, we used the same ensemble of model simulations (see section 4.1; Table 1) to investigate changes in mean annual precipitation (MAP) at Cobham (UK) for two PETM-type scenarios (i.e. doubling or tripling of CO_2; Fig. 4b). For a tripling of CO_2, modelling simulations indicate stable (e.g. HadCM3L) or decreasing MAP (22%; e.g. HadCM3L-I2). For a doubling of CO_2, model simulations indicate increasing (6 to 7 %; CCSM3-H, HadCM3L-C), stable (e.g. HadCM3L) or decreasing MAP (5 to 22%; HadCM3L-I, CCSM3-W). A decrease in MAP is inconsistent with proxy evidence at Cobham. However, model simulations run at hourly resolution (i.e. HadCM3L-C) also show a change in precipitation extremes at Cobham for a doubling of CO_2, with an increase in the 90th percentile storm extreme rate (+7%; HadCM3L-C). This indicates an increase towards more intense rainfall events. Furthermore, an increase in tail width (+28%), indicates more frequent heavy rainfall events of a given size (Carmichael et al., 2018). Decoupling between MAP and extreme events has previously been noted for other mid-to-low latitude PETM settings (e.g. Tunisia, Tanzania; Carmichael et al. 2018) and should be considered in future proxy-model comparisons.

Geochemical and botanical proxies at other sites also provide further evidence for enhanced rainfall in northern Europe during the PETM, with evidence for an increase in wetland-type environments in northern France (Garel et al., 2013) and other parts of the region surrounding the North Sea (Eldrett et al., 2014; Kender et al., 2012). There is also evidence for abundant low-salinity tolerant dinocysts (Sluijs et al., 2007), enhanced clay mineral deposition (Bornemann et al., 2014) and isotopically-

437 depleted tooth apatite $\delta^{18}O$ values (Myhre et al., 1995) within North Sea marine
438 sediments, all of which indicate wetter conditions during the PETM. This indicates a
439 shift towards wetter conditions in northern Europe during the PETM and perhaps an
440 increase in the occurrence of extreme rainfall events (Carmichael et al., 2018). In
441 these settings, terrestrial biomarker proxies may be subject to additional controls (e.g.
442 pH, hydrology and/or the presence of open water areas) and should therefore be
443 interpreted within a multi-proxy framework.
444

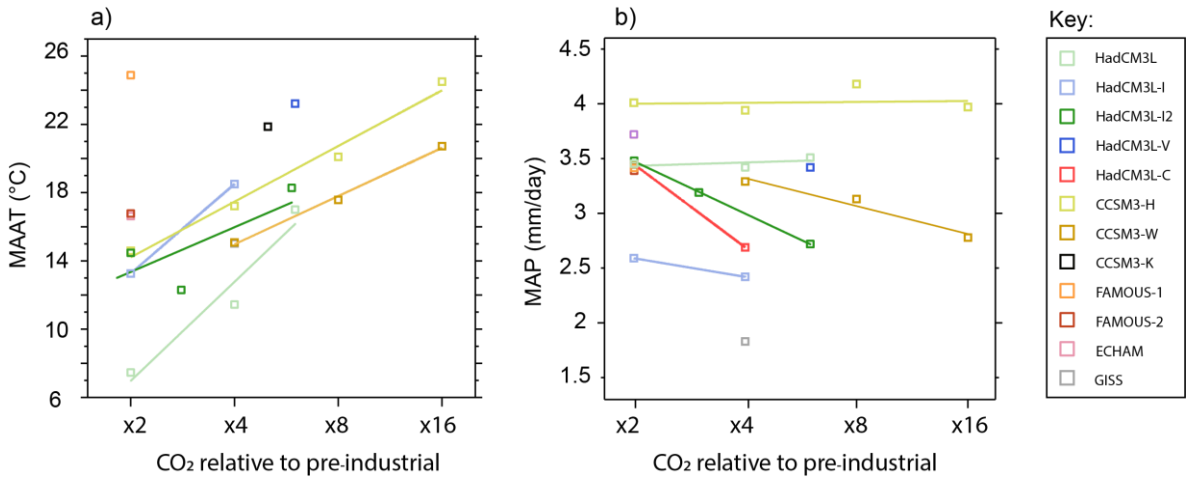

Figure 4. Model-derived mean annual surface temperature and precipitation estimates as a function of CO_2 at Cobham (UK). Simulations represent the mid-point of the most appropriate geological stage (Ypresian; 56 to 47.8 Ma). For full details on each model simulation, see Supplementary Information. (For interpretation of the references to color in this figure legend, the reader is referred to the web version of this article.)

445

446 **5. Conclusions**

447 Here we have reconstructed terrestrial paleoenvironmental change within the Cobham
448 Lignite Bed, which spans the very latest Paleocene, onset and early part of the PETM.
449 Proxies indicate high terrestrial temperatures prior to the PETM (22 to 26°C),

consistent with model simulations. However, inconsistent with local, regional and global evidence, the biomarker proxies seem to indicate significant cooling during the onset and early PETM (ca. 5 to 11°C). We attributed this to enhanced waterlogging and the development of a persistent peatland with areas of open water, biasing the brGDGT paleothermometer. This study implies the need for care when applying biomarker-based temperature proxies in transitional terrestrial environments (e.g. mire settings). It also serves as a cautionary tale on the danger of attempting to interpret proxy records without a wider understanding of the environmental context, especially the pH and the hydrology.

Acknowledgements

This research was funded through the advanced ERC grant 'The Greenhouse Earth System' (T-GRES. Project reference: 340923). RDP also acknowledges the Royal Society Wolfson Research Merit Award and funding from the NERC. BDAN acknowledges additional funding from a Royal Society Tata University Research Fellowship. We thank the NERC Life Sciences Mass Spectrometry Facility (Bristol) for analytical support. A.F., D.J.L. and R.D.P acknowledge funding from NERC through NE/K014757/1, NE/I005722/1, NE/I005714/1, and (PJV also) NE/P013805/1. We gratefully acknowledge funding to M.E.C. from NERC grant NE/J008656/1 and to R.D.P. from NERC grant NE/J008591/1. M.E.C. thanks the Leverhulme Trust for providing funding (Grant number F/07/537/0); Alfred McAlpine, AMEC and Channel Tunnel Rail Link for access to the Cobham site.

Data availability

Data can be accessed via the online supporting information, via http://www.pangaea.de/, or from the author (email: gordon.inglis@bristol.ac.uk).

References

Aze, T., Pearson, P.N., Dickson, A.J., Badger, M.P.S., Bown, P.R., Pancost, R.D., Gibbs, S.J., Huber, B.T., Leng, M.J., Coe, A.L., Cohen, A.S. and Foster, G.L. (2014) Extreme warming of tropical waters during the Paleocene–Eocene Thermal Maximum. Geology.42. 739-742

Bornemann, A., Norris, R.D., Lyman, J.A., D'Haenens, S., Groeneveld, J., Röhl, U., Farley, K.A. and Speijer, R.P. (2014) Persistent environmental change after the Paleocene–Eocene Thermal Maximum in the eastern North Atlantic. Earth and Planetary Science Letters 394, 70-81.

Carmichael, M.J., Inglis, G.N., Badger, M.P., Naafs, B.D.A., Behrooz, L., Remmelzwaal, S., Monteiro, F.M., Rohrssen, M., Farnsworth, A., Buss, H.L. Dickson, A.J, Valdes, P.J., Lunt, D.J and Pancost, R.D. (2017) Hydrological and associated biogeochemical consequences of rapid global warming during the Paleocene-Eocene Thermal Maximum. *Global and Planetary Change*, 157,114-138.

Carmichael, M.J., Pancost, R.D., Lunt, D. (2018) Changes in the occurrence of extreme precipitation events at the Paleocene–Eocene thermal maximum. Global and Planetary Change. 501, 24-36.

Colcord, D.E., Cadieux, S.B., Brassell, S.C., Castañeda, I.S., Pratt, L.M. and White, J. (2015) Assessment of branched GDGTs as temperature proxies in sedimentary records from several small lakes in southwestern Greenland. Organic Geochemistry. 82, 33-41.

Collinson, M., Hooker, J. and Grocke, D. (2003) Cobham lignite bed and penecontemporaneous macrofloras of southern England: A record of vegetation and fire across the Paleocene-Eocene Thermal Maximum. Special Papers - Geological Society of American, 333-350.

Collinson, M.E., Smith, S.Y., van Konijnenburg-van Cittert, J.H., Batten, D.J., van der Burgh, J., Barke, J. and Marone, F. (2013) New observations and synthesis of Paleogene heterosporous water ferns. International Journal of Plant Sciences.174, 350-363.

Collinson, M.E., Steart, D.C., Harrington, G.J., Hooker, J.J., Scott, A.C., Allen, L.O., Glasspool, I.J. and Gibbons, S.J. (2009) Palynological evidence of vegetation dynamics in response to palaeoenvironmental change across the onset of the Paleocene-Eocene Thermal Maximum at Cobham, Southern England. Grana 48, 38-66.

Currano, E.D., Wilf, P., Wing, S.L., Labandeira, C.C., Lovelock, E.C. and Royer, D.L.. (2008) Sharply increased insect herbivory during the Paleocene–Eocene Thermal Maximum. PNAS 105, 1960-1964.

Damsté, J.S.S., Rijpstra, W.I.C., Foesel, B.U., Huber, K.J., Overmann, J., Nakagawa, S., Kim, J.J., Dunfield, P.F., Dedysh, S.N. and Villanueva, (2018) An overview of the occurrence of ether-and ester-linked iso-diabolic acid membrane lipids in microbial cultures of the Acidobacteria: Implications for brGDGT paleoproxies for temperature and pH. Organic Geochemistry. 124, 63-76.

De Jonge, C., Hopmans, E.C., Zell, C.I., Kim, J.-H., Schouten, S. and Sinninghe Damsté, J.S. (2014) Occurrence and abundance of 6-methyl branched glycerol dialkyl glycerol tetraethers in soils: Implications for palaeoclimate reconstruction. Geochimica et Cosmochimica Acta 141, 97-112.

Dickson, A.J., Cohen, A.S., Coe, A.L., Davies, M., Shcherbinina, E.A. and Gavrilov, Y.O. (2015) Evidence for weathering and volcanism during the PETM from

523 Arctic Ocean and Peri-Tethys osmium isotope records. Palaeogeography,
524 Palaeoclimatology, Palaeoecology 438, 300-307.
525 Eldrett, J., Greenwood, D., Polling, M., Brinkhuis, H. and Sluijs, A. (2014) A seasonality
526 trigger for carbon injection at the Paleocene–Eocene Thermal Maximum.
527 Climate of the Past 10, 759-769.
528 Fricke, H.C. and Wing, S.L. (2004) Oxygen isotope and paleobotanical estimates of
529 temperature and $\delta^{18}O$–latitude gradients over North America during the early
530 Eocene. American Journal of Science 304, 612-635.
531 Frieling, J., Gebhardt, H., Huber, M., Adekeye, O.A., Akande, S.O., Reichart, G.-J.,
532 Middelburg, J.J., Schouten, S. and Sluijs, A. (2017) Extreme warmth and heat-
533 stressed plankton in the tropics during the Paleocene-Eocene Thermal
534 Maximum. Science Advances 3, e1600891.
535 Frieling, J., Iakovleva, A.I., Reichart, G.-J., Aleksandrova, G.N., Gnibidenko, Z.N.,
536 Schouten, S. and Sluijs, A. (2014) Paleocene–Eocene warming and biotic
537 response in the epicontinental West Siberian Sea. Geology 42, 767-770.
538 Garel, S., Schnyder, J., Jacob, J., Dupuis, C., Boussafir, M., Le Milbeau, C., Storme,
539 J.-Y., Iakovleva, A.I., Yans, J., Baudin, F., Fléhoc, C. and Quesnel, F. (2013)
540 Paleohydrological and paleoenvironmental changes recorded in terrestrial
541 sediments of the Paleocene–Eocene boundary (Normandy, France).
542 Palaeogeography, Palaeoclimatology, Palaeoecology 376, 184-199.
543 Gehler, A., Gingerich, P.D. and Pack, A. (2016) Temperature and atmospheric CO_2
544 concentration estimates through the PETM using triple oxygen isotope analysis
545 of mammalian bioapatite. Proceedings of the National Academy of Sciences
546 113, 7739-7744.
547 Gutjahr, M., Ridgwell, A., Sexton, P.F., Anagnostou, E., Pearson, P.N., Pälike, H.,
548 Norris, R.D., Thomas, E. and Foster, G.L. (2017) Very large release of mostly
549 volcanic carbon during the Palaeocene–Eocene Thermal Maximum. 548, 573.
550 Handley, L., O'Halloran, A., Pearson, P.N., Hawkins, E., Nicholas, C.J., Schouten, S.,
551 McMillan, I.K. and Pancost, R.D. (2012) Changes in the hydrological cycle in
552 tropical East Africa during the Paleocene–Eocene Thermal Maximum.
553 Palaeogeography, Palaeoclimatology, Palaeoecology 329, 10-21.
554 Hollis, C.J., Dunkley Jones, T., Anagnostou, E., Bijl, P.K., Cramwinckel, M.J., Cui, Y.,
555 Dickens, G.R., Edgar, K.M., Eley, Y., Evans, D., Foster, G.L., Frieling, J., Inglis,
556 G.N., Kennedy, E.M., Kozdon, R., Lauretano, V., Lear, C.H., Littler, K., Meckler,
557 N., Naafs, B.D.A., Pälike, H., Pancost, R.D., Pearson, P., Royer, D.L.,
558 Salzmann, U., Schubert, B., Seebeck, H., Sluijs, A., Speijer, R., Stassen, P.,
559 Tierney, J., Tripati, A., Wade, B., Westerhold, T., Witkowski, C., Zachos, J.C.,
560 Zhang, Y.G., Huber, M. and Lunt, D.J. (2019) The DeepMIP contribution to
561 PMIP4: methodologies for selection, compilation and analysis of latest
562 Paleocene and early Eocene climate proxy data, incorporating version 0.1 of
563 the DeepMIP database. Geosci. Model Dev. Discuss. 2019, 1-98.
564 Hopmans, E.C., Schouten, S. and Damsté, J.S.S. (2016) The effect of improved
565 chromatography on GDGT-based palaeoproxies. Organic Geochemistry 93, 1-
566 6.
567 Huguet, A., Grossi, V., Belmahdi, I., Fosse, C. and Derenne, S. (2015) Archaeal and
568 bacterial tetraether lipids in tropical ponds with contrasting salinity
569 (Guadeloupe, French West Indies): Implications for tetraether-based
570 environmental proxies. Organic Geochemistry. 83, 158-169.
571 Inglis, G.N., Collinson, M.E., Riegel, W., Wilde, V., Farnsworth, A., Lunt, D.J., Valdes,
572 P., Robson, B.E., Scott, A.C., Lenz, O.K., Naafs, B.D.A. and Pancost, R.D.

(2017) Mid-latitude continental temperatures through the early Eocene in western Europe. Earth and Planetary Science Letters 460, 86-96.

Inglis, G.N., Naafs, B.D.A., Zheng, Y., McClymont, E.L., Evershed, R.P. and Pancost, R.D. (2018) Distributions of geohopanoids in peat: Implications for the use of hopanoid-based proxies in natural archives. Geochimica et Cosmochimica Acta 224, 249-261.

Jaramillo, C., Ochoa, D., Contreras, L., Pagani, M., Carvajal-Ortiz, H., Pratt, L.M., Krishnan, S., Cardona, A., Romero, M., Quiroz, L., Rodriguez, G., Rueda, M.J., de la Parra, F., Morón, S., Green, W., Bayona, G., Montes, C., Quintero, O., Ramirez, R., Mora, G., Schouten, S., Bermudez, H., Navarrete, R., Parra, F., Alvarán, M., Osorno, J., Crowley, J.L., Valencia, V. and Vervoort, J. (2010) Effects of Rapid Global Warming at the Paleocene-Eocene Boundary on Neotropical Vegetation. Science 330, 957-961.

John, C.M., Bohaty, S.M., Zachos, J.C., Sluijs, A., Gibbs, S., Brinkhuis, H. and Bralower, T. (2008) North American continental margin records of the Paleocene-Eocene thermal maximum: Implications for global carbon and hydrological cycling. Paleoceanography. 23.

Jones, T.D., Lunt, D.J., Schmidt, D.N., Ridgwell, A., Sluijs, A., Valdes, P.J. and Maslin, M.. (2013) Climate model and proxy data constraints on ocean warming across the Paleocene–Eocene Thermal Maximum. Earth Science Reviews. 125, 123-145.

Kender, S., Stephenson, M.H., Riding, J.B., Leng, M.J., Knox, R.W.B., Peck, V.L., Kendrick, C.P., Ellis, M.A., Vane, C.H. and Jamieson, R. (2012) Marine and terrestrial environmental changes in NW Europe preceding carbon release at the Paleocene–Eocene transition. Earth and Planetary Science Letters 353, 108-120.

Kiehl, J.T. and Shields, C.A. (2013) Sensitivity of the Palaeocene–Eocene Thermal Maximum climate to cloud properties. Philosophical Transactions of the Royal Society of London A: Mathematical, Physical and Engineering Sciences 371, 20130093.

Lunt, D.J., Dunkley Jones, T., Heinemann, M., Huber, M., LeGrande, A., Winguth, A., Loptson, C., Marotzke, J., Roberts, C.D., Tindall, J., Valdes, P. and Winguth, C. (2012) A model–data comparison for a multi-model ensemble of early Eocene atmosphere–ocean simulations: EoMIP. Clim. Past 8, 1717-1736.

Lunt, D.J., Farnsworth, A., Loptson, C., Foster, G.L., Markwick, P., O'Brien, C.L., Pancost, R.D., Robinson, S.A. and Wrobel, N. (2016) Palaeogeographic controls on climate and proxy interpretation. Climate of the Past 12, 1181-1198.

McInerney, F.A. and Wing, S.L. (2011) The Paleocene-Eocene Thermal Maximum: A perturbation of carbon cycle, climate, and biosphere with implications for the future. Annual Review of Earth and Planetary Sciences 39, 489-516.

Myhre, A., Thiede, J. and Firth, J. (1995) Shipboard Scientific Party, Initial Reports: sites 907–913, North Atlantic-Arctic Gateways. Proceedings, Initial Reports, Ocean Drilling Program 151, 926.

Naafs, B.D.A., Inglis, G.N., Zheng, Y., Amesbury, M.J., Biester, H., Bindler, R., Blewett, J., Burrows, M.A., del Castillo Torres, D., Chambers, F.M., Cohen, A.D., Evershed, R.P., Feakins, S.J., Gałka, M., Gallego-Sala, A., Gandois, L., Gray, D.M., Hatcher, P.G., Honorio Coronado, E.N., Hughes, P.D.M., Huguet, A., Könönen, M., Laggoun-Défarge, F., Lähteenoja, O., Lamentowicz, M., Marchant, R., McClymont, E., Pontevedra-Pombal, X., Ponton, C., Pourmand, A., Rizzuti, A.M., Rochefort, L., Schellekens, J., De Vleeschouwer, F. and

623 Pancost, R.D. (2017) Introducing global peat-specific temperature and pH
624 calibrations based on brGDGT bacterial lipids. Geochimica et Cosmochimica
625 Acta 208, 285-301.
626 Naafs, B., McCormick, D., Inglis, G. and Pancost, R.. (2018a) Archaeal and bacterial
627 H-GDGTs are abundant in peat and their relative abundance is positively
628 correlated with temperature. Geochimica et Cosmochimica Acta. 227, 156-170.
629 Naafs, B.D.A., Rohrssen, M., Inglis, G.N., Lähteenoja, O., Feakins, S.J., Collinson,
630 M.E., Kennedy, E.M., Singh, P.K., Singh, M.P., Lunt, D.J. and Pancost, R.D.
631 (2018b). High temperatures in the terrestrial mid-latitudes during the early
632 Palaeogene. *Nature Geoscience*, 11, 766.
633 Pancost, R.D., Baas, M., van Geel, B. and Sinninghe Damsté, J.S. (2003) Response
634 of an ombrotrophic bog to a regional climate event revealed by macrofossil,
635 molecular and carbon isotopic data. The Holocene 13, 921-932.
636 Pancost, R.D., Steart, D.S., Handley, L., Collinson, M.E., Hooker, J.J., Scott, A.C.,
637 Grassineau, N.V. and Glasspool, I.J. (2007) Increased terrestrial methane
638 cycling at the Palaeocene–Eocene thermal maximum. Nature 449, 332-335.
639 Ravizza, G., Norris, R., Blusztajn, J., Aubry, M (2001) An osmium isotope excursion
640 associated with the late Paleocene thermal maximum: Evidence of intensified
641 chemical weathering. Paleoceanography 16, 155-163.
642 Sachse, D., Billault, I., Bowen, G.J., Chikaraishi, Y., Dawson, T.E., Feakins, S.J.,
643 Freeman, K.H., Magill, C.R., McInerney, F.A. and Van der Meer, M.T. (2012)
644 Molecular paleohydrology: interpreting the hydrogen-isotopic composition of
645 lipid biomarkers from photosynthesizing organisms. Annual Review of Earth
646 and Planetary Sciences. 40. 221-249.
647 Sagoo, N., Valdes, P., Flecker, R. and Gregoire, L.J. (2013) The Early Eocene equable
648 climate problem: can perturbations of climate model parameters identify
649 possible solutions? Philosophical Transactions of the Royal Society A:
650 Mathematical, Physical and Engineering Sciences. 371.
651 Schmitz, B. and Pujalte, V. (2007) Abrupt increase in seasonal extreme precipitation
652 at the Paleocene-Eocene boundary. Geology 35, 215-218.
653 Schoon, P.L., Heilmann-Clausen, C., Schultz, B.P., Damsté, J.S.S. and Schouten, S.
654 (2015) Warming and environmental changes in the eastern North Sea Basin
655 during the Palaeocene–Eocene Thermal Maximum as revealed by biomarker
656 lipids. Organic Geochemistry 78, 79-88.
657 Schouten, S., Woltering, M., Rijpstra, W.I.C., Sluijs, A., Brinkhuis, H. and Sinninghe
658 Damsté, J.S. (2007) The Paleocene–Eocene carbon isotope excursion in
659 higher plant organic matter: Differential fractionation of angiosperms and
660 conifers in the Arctic. Earth and Planetary Science Letters 258, 581-592.
661 Secord, R., Bloch, J.I., Chester, S.G., Boyer, D.M., Wood, A.R., Wing, S.L., Kraus,
662 M.J., McInerney, F.A. and Krigbaum, J.J.S. (2012) Evolution of the earliest
663 horses driven by climate change in the Paleocene-Eocene Thermal Maximum.
664 Science. 335, 959-962.
665 Secord, R., Gingerich, P.D., Lohmann, K.C. and MacLeod, K.G. (2010) Continental
666 warming preceding the Palaeocene-Eocene thermal maximum. Nature 467,
667 955-958.
668 Sluijs, A., Bijl, P., Schouten, S., Röhl, U., Reichart, G.-J. and Brinkhuis, H. (2011)
669 Southern ocean warming, sea level and hydrological change during the
670 Paleocene-Eocene thermal maximum. Climate of the Past 7. 47-61
671 Sluijs, A., Brinkhuis, H., Schouten, S., Bohaty, S.M., John, C.M., Zachos, J.C.,
672 Reichart, G.-J., Damsté, J.S.S., Crouch, E.M. and Dickens, G.R. (2007)

673 Environmental precursors to rapid light carbon injection at the
674 Palaeocene/Eocene boundary. Nature 450, 1218-1221.
675 Sluijs, A., Schouten, S., Pagani, M., Woltering, M., Brinkhuis, H., Damsté, J.S.S.,
676 Dickens, G.R., Huber, M., Reichart, G.-J. and Stein, R. (2006) Subtropical Arctic
677 Ocean temperatures during the Palaeocene/Eocene thermal maximum. Nature
678 441, 610-613.
679 Sluijs, A., van Roij, L., Harrington, G.J., Schouten, S., Sessa, J.A., LeVay, L.J.,
680 Reichart, G.J. and Slomp, C.P. (2014) Warming, euxinia and sea level rise
681 during the Paleocene–Eocene Thermal Maximum on the Gulf Coastal Plain:
682 implications for ocean oxygenation and nutrient cycling. Climate of the Past. 10,
683 1421-1439.
684 Smith, J.J., Hasiotis, S.T., Kraus, M.J. and Woody, D. (2009) Transient dwarfism of
685 soil fauna during the Paleocene–Eocene Thermal Maximum. Proceedings of
686 the National Academy of Sciences 106.42. 17655-17660.
687 Tierney, J.E., Russell, J.M., Eggermont, H., Hopmans, E., Verschuren, D. and
688 Damsté, J.S.J.G.e.C.A. (2010) Environmental controls on branched tetraether
689 lipid distributions in tropical East African lake sediments. Geochimica et
690 Cosmochimica Acta. 74, 4902-4918.
691 Tierney, J.E. and Russell, J.M (2009) Distributions of branched GDGTs in a tropical
692 lake system: implications for lacustrine application of the MBT/CBT paleoproxy.
693 Organic Geochemistry. 40, 1032-1036.
694 Tripati, A. and Elderfield, H. (2005) Deep-Sea Temperature and Circulation Changes
695 at the Paleocene-Eocene Thermal Maximum. Science 308, 1894-1898.
696 Valdes, P.J., Armstrong, E., Badger, M.P., Bradshaw, C.D., Bragg, F., Davies-
697 Barnard, T., Day, J.J., Farnsworth, A., Hopcroft, P.O., Kennedy, A.T. and Lord,
698 N.S. (2017). The BRIDGE HadCM3 family of climate models: HadCM3@ Bristol
699 v1. 0. *Geoscientific Model Development*, 10, 3715-3743.
700 Weber, Y., Damsté, J.S.S., Zopfi, J., De Jonge, C., Gilli, A., Schubert, C.J., Lepori, F.,
701 Lehmann, M.F. and Niemann, H (2018) Redox-dependent niche differentiation
702 provides evidence for multiple bacterial sources of glycerol tetraether lipids in
703 lakes. Proceedings of the National Academy of Sciences . 115, 10926-10931.
704 Weijers, J.W.H., Schouten, S., van der Linden, M., van Geel, B. and Sinninghe
705 Damsté, J.S. (2004) Water table related variations in the abundance of intact
706 archaeal membrane lipids in a Swedish peat bog. FEMS Microbiology Letters.
707 239. 51-56.
708 Weijers, J.W., Schouten, S., van den Donker, J.C., Hopmans, E.C. and Damsté,
709 J.S.S., (2007). Environmental controls on bacterial tetraether membrane lipid
710 distribution in soils. *Geochimica et Cosmochimica Acta*, 71, 703-713.
711 Weijers, J.W., Steinmann, P., Hopmans, E.C., Schouten, S. and Damsté, J.S.S.
712 (2011) Bacterial tetraether membrane lipids in peat and coal: Testing the MBT–
713 CBT temperature proxy for climate reconstruction. *Organic Geochemistry*, 42,
714 477-486.
715 Wing, S.L., Harrington, G.J., Smith, F.A., Bloch, J.I., Boyer, D.M. and Freeman, K.H.
716 (2005) Transient Floral Change and Rapid Global Warming at the Paleocene-
717 Eocene Boundary. Science 310, 993-996.
718 Yang, H., Lü, X., Ding, W., Lei, Y., Dang, X. and Xie, S. (2015) The 6-methyl branched
719 tetraethers significantly affect the performance of the methylation index (MBT′)
720 in soils from an altitudinal transect at Mount Shennongjia. Organic
721 Geochemistry. 82, 42-53.

722 Zachos, J.C., Dickens, G.R. and Zeebe, R.E. (2008) An early Cenozoic perspective
723 on greenhouse warming and carbon-cycle dynamics. Nature 451, 279-283.
724 Zachos, J.C., Schouten, S., Bohaty, S., Quattlebaum, T., Sluijs, A., Brinkhuis, H.,
725 Gibbs, S. and Bralower, T. (2006) Extreme warming of mid-latitude coastal
726 ocean during the Paleocene-Eocene Thermal Maximum: Inferences from TEX_{86}
727 and isotope data. Geology 34, 737-740.
728 Zink, K.-G., Vandergoes, M.J., Mangelsdorf, K., Dieffenbacher-Krall, A.C. and
729 Schwark, L.J.O.G. (2010) Application of bacterial glycerol dialkyl glycerol
730 tetraethers (GDGTs) to develop modern and past temperature estimates from
731 New Zealand lakes. Organic Geochemistry. 41, 1060-1066.

732